

Citation for published version:
Wang, Q, Bowen, CR, Lewis, R, Chen, J, Lei, W, Zhang, H, Li, MY & Jiang, S 2019, 'Hexagonal boron nitride nanosheets doped pyroelectric ceramic composite for high-performance thermal energy harvesting', *Nano* Energy, vol. 60, pp. 144-152. https://doi.org/10.1016/j.nanoen.2019.03.037

10.1016/j.nanoen.2019.03.037

Publication date: 2019

Document Version Peer reviewed version

Link to publication

Publisher Rights CC BY-NC-ND

University of Bath

Alternative formats

If you require this document in an alternative format, please contact: openaccess@bath.ac.uk

General rights

Copyright and moral rights for the publications made accessible in the public portal are retained by the authors and/or other copyright owners and it is a condition of accessing publications that users recognise and abide by the legal requirements associated with these rights.

If you believe that this document breaches copyright please contact us providing details, and we will remove access to the work immediately and investigate your claim.

Download date: 07, Mar. 2023

Hexagonal boron nitride nanosheets doped pyroelectric ceramic composite for high-performance thermal energy harvesting

Qingping Wang^{a,b}, Chris R. Bowen^c, Rhodri Lewis^c, Jun Chen^d, Wen Lei^a, Haibo Zhang^e, Ming-Yu Li^{a*}, and Shenglin Jiang^{a*}

^a School of Optical and Electronic Information, Huazhong University of Science and Technology, Wuhan 430074, P. R. China

^b Department of Physics & Mechanical and Electronic Engineering, Hubei University of Education, Wuhan 430205, P. R. China

^c Department of Mechanical Engineering, University of Bath, Claverton Down Road, Bath BA2 7AY, UK

^d Department of Materials Science and Engineering, Stanford University, Stanford, California 94305, USA

^e College of Materials Science and Engineering, State Key Laboratory of Material Processing and Die & Mould Technology, Huazhong University of Science and Technology, Wuhan 430074, P. R. China

Corresponding authors at: School of Optical and Electronic Information, Huazhong University of Science and Technology, Wuhan 430074, P. R. China E-mail addresses: mingyuli.oliver@gmail.com (M. Li), jslhust@gmail.com (S. Jiang).

Abstract: Recently, recycling energy from wasted heat with pyroelectric materials has received significant attention. However, pyroelectric energy harvesters generally suffer from a low energy efficiency due to the low rates of heat transfer. Here, we report high-performance thermal energy harvesting using novel hybrid pyroelectric ceramics with greatly improved heat transfer and rate of temperature changes. This is achieved by evenly dispersing 0.1 wt.% hexagonal boron nitride (hBN) nanosheets into a Pb[(Mn1/3Nb2/3)1/2(Mn1/3Sb2/3)1/2]0.04(Zr0.95Ti0.05)0.96O3 (lead magnesium niobate-lead antimony-manganese-lead zirconate titanate: PMN-PMS-PZT) ceramic matrix. Due to the vibrations of whole chain and phonon scattering, heat transfer through the hybrid crystalline chain is more efficient than that of unfilled PMN-PMS-PZT. It is demonstrated that the harvested power was increased by up to 65.6%. This work paved an efficient and cost-effective way to largely improve the traditional pyroelectric ceramic for thermal energy harvesting.

Key words: Hexagonal boron nitride, Pyroelectric ceramic, Thermal conductivity,
Thermal energy harvesting

1. Introduction

With the threat of global warming and energy crisis, the search for renewable energy resources with reduced carbon emissions is one of the most urgent challenges to the sustainable development of human civilization [1-6]. Thermal energy is a form of clean energy form with a collection of compelling features: indispensability, ubiquity, abundantly available and delivering highest available work. Thermal energy can be generated in a wide variety of energy conversion processes [7-13]. The ability to use the pyroelectric effect to generate electricity from wasted thermal energy and temperature fluctuations and transients has attracted a wide-range of interest in both the scientific community and industry [14-22].

To improve the performance of pyroelectric generators, firstly, much effort has been committed to enhance the materials pyroelectric coefficient [23-26] to improve the charge generated for a given temperature change. Secondly, partial efforts from the community have been made in an attempt to increase the rate of temperature change dT/dt and thereby increase the generated current. This approach was usually realized by fabricating a meshed or partially covered electrodes on pyroelectric materials, such as PZT [27-30], PVDF [31] and ZnO [32]. Thirdly, the ability to simultaneously enhance both the pyroelectric coefficient and the rate of temperature change of a material is an effective approach to improve the energy harvesting performance [23]. However, the output power of the pyroelectric devices is still relatively low for practical applications. Recently, the development of fillers with high thermal conductivity and electrical resistivity was reported as an efficient approach to enhance the thermal

transfer of ceramics [33, 34], and thereby achieved greatly improved the thermal energy harvesting performance. Typical high thermal conductivity fillers include diamond, beryllium oxide (BeO), aluminum nitride (AlN), aluminum oxide (Al₂O₃), and boron nitride (BN) [35, 36]. However, a number of these fillers have challenges associated with their high cost [23], material toxicity [33] and instability in ambient environment [34]. In addition, for Al based fillers, such as AlN, the atoms can stack at the grain boundaries of the ceramic matrix due to the relatively higher atomic mass, which in turn can restrict the thermal transfer as a result of the limited thermal conduction of the interfaces between grain boundaries compared to the grain interior.

Bearing these points in mind, we have selected BN as a dopant which is low-cost, non-toxic, and chemically stable together with lower atomic mass [37] and designed a high-performance pyroelectric hybrid ceramic by utilizing two-step sintering method. Initially, utilized we solid-state reaction method prepare $Pb[(Mn_{1/3}Nb_{2/3})_{1/2}(Mn_{1/3}Sb_{2/3})_{1/2}]_{0.04}(Zr_{0.95}Ti_{0.05})_{0.96}O_3(PMN-PMS-PZT)$ ceramics. The prepared PMN-PMS-PZT powders and commercial hBN nanosheets were then mixed to fabricate hybrid pyroelectric ceramics by the same reaction technique. Furthermore, compared to the pristine sample, the sample with 0.1 wt.% hBN exhibited an enhanced performance, including an improved pyroelectric coefficient by 16.2%, an enhanced thermal conductivity by 12.5% and a higher rate of temperature change, dT/dt, by 8.2%. Finally, an energy harvesting system subjected to temperature cycling was designed to assess the output voltage of the energy harvester and was demonstrated to achieve a 65.6% increase in harvesting power compared to that of the device with the unfilled PMN-PMS-PZT ceramic. Our work represents a new approach in designing strategies and experimental methods to achieve high heat transfer for pyroelectric energy harvesting applications.

2. Experimental section

2.1. Sample preparation

The PMN-PMS-PZT powders were initially prepared by a method described in our earlier work [24]. Based on the different ratios of oxides, PbO (99.0%), ZrO₂ (99.5%), TiO₂ (99.8%), Nb₂O₅ (99.5%), Sb₂O₃ (99.0%), and Mn(NO₃)₂ (50%, all from Sinopharm Chemical Reagent Co., Ltd, China), were stoichiometrically weighed and ball milled in deionized (DI) water for 4 h. After heating in a furnace at 100 °C for 1 h, the dry slurries were calcined at 900 °C for 3 h with a ramp rate of 5 °C/min, and then ground by hand and ball milled again in DI water for 4 h, followed by drying. The powders were sintered in covered alumina crucibles at 1230 °C for 4 h and cooled in air. The resulting PMN-PMS-PZT powders exhibited a high degree of crystallinity and pure perovskite phase, as observed in Fig. S1a and Fig. S1b.

Subsequently, the PMN-PMS-PZT powders and the commercial hBN nanosheets (99%, from Aladdin) were mixed according to the formula of PMN-PMS-PZT: xhBN with x=0, 0.1, 0.2, and 0.3 wt.%. The hBN nanosheets had a hexagonal crystal structure [33] with a plate-like morphology, as shown in Fig. S1c and Fig. S1d. After ball milling in DI water for 4 h, each mixture was pressed into a disk with a diameter of 10 mm under 8 MPa using 6 wt.% polyvinyl acetate (PVA) as a binder. Sintering was carried out in covered alumina crucibles at 1070~1170 °C for 2 h in air with a rapid ramping

rate of 8 °C/min, followed by the natural cooling.

2.2. Crystal structure analysis and morphology characterization

The crystal structure of the resulting samples was characterized by using a X'Pert-PRO diffractometer with Cu Kα radiation (PANalytical, Holland). The surface morphology and element analysis were obtained by field-emission scanning electron microscopy (FE-SEM Sirion200, FEI, USA) and energy-dispersive X-ray spectroscopy (EDS) respectively. The elemental distribution was examined with an electron probe micro analyzer (EPMA-8050G, SHIMADZU, Japan). The Raman spectra of the samples were recorded with a Vertex spectrometer from Bruker Co. (Bremen, Germany).

2.3. Electrical property measurements

For electrical property characterization, samples with a diameter of ~ 8.5 mm were mechanically polished to ~ 0.31 mm in thickness. Subsequently, each sample was printed with Ag electrodes on both sides by silk-screen printing and treated with a 600 °C heating process for 25 min. The relative permittivity (ϵ_r) and loss tangent (tan δ) of each sample were measured using an impedance analyzer (HP4294A, Agilent Technologies, USA) at several frequencies in a temperature range from 30 to 300 °C. The ferroelectric properties were measured at 10 Hz by a polarization and ferroelectric test system (CPE1601, PolyK Technologies, and USA). Prior to assessing the pyroelectric properties, samples were poled under an applied electric field at elevated temperature (3 kV/mm, 25 min, 120 °C). The pyroelectric short circuit current was measured by an electrometer (Picoammeter 6485, Keithley Instruments, Cleveland,

OH), and the pyroelectric coefficient was evaluated using a standard Byer-Roundy method via an in-house pyroelectric parameter tracer.

2.4. Measurement of thermal conductivity

The thermal diffusivity (α) and specific heat capacity (C_p) of the samples were measured by a graphite-coated cylindrical specimen with an average thickness of 1 mm and a diameter of 12.7 mm from 20 to 60 °C by laser flash analysis using a LFA427 Microflash (NETZSCH-Gerätebau GmbH, Germany). The density of the samples (ρ) were characterized by the Archimedes method [38]. The thermal conductivity (K) was calculated from $K = \alpha \rho C_p$ [39].

2.5. Measurement of pyroelectric energy harvester

Two Peltier cells were employed to provide a temperature variation (dT/dt) for the harvester. The temperature of the hot/cold flow was simultaneously monitored with two K-type thermocouples, and adjusted with a heat sink and fan. The pyroelectric signals from the harvester were recorded with a data acquisition system set up based on LABVIEW.

3. Results and Discussion

The evolution of the crystal structures and surface morphologies of the PMN-PMS-PZT samples with a variation of hBN content were shown in Fig. S2 and Fig. 1. X-ray diffraction (XRD) patterns of each sample is shown in Fig. S2a, and the enlarged XRD patterns in the 2θ angle of 28.0-28.8° is presented in Fig. S2b. The surface morphologies of the samples are shown in Fig. 1a, b and Fig. S2c, d, and the average

grain size and density are summarized in Fig. S2e, f. Generally, the existence of high thermal conductivity hBN can promote the formation of a hybrid pyroelectric ceramic, resulting in a noticeable morphological evolution of PMN-PMS-PZT ceramics as a function of hBN content. In particular, as observed via the X-ray diffraction (XRD) patterns in Figure S2a, the presence of (001), (100), (110), (111), (200), (210), (211), (220), (300), and (310) peaks suggests that the crystallization of a pure perovskite phase [24] without any formation of the pyrochlore phase. In particular, a peak at 28.15° was observed in samples with 0 wt.% and 0.1 wt.% hBN, as shown in Figure S2b, which is a result of the existence of the PbO secondary phase. With a further increase in hBN content, the PbO peak disappeared, indicating that hBN can promote the formation of a hybrid pyroelectric ceramic and inhibit the formation of a PbO phase. In addition, as shown in Fig. 1a, b, the quality of the ceramics was improved with less defects compared to the pristine PMN-PMS-PZT with no added hBN filler in the composite sample, which can be ascribed to enhanced crystallization when B and N ions entered into the lattice [40]. However, with a further increase in hBN addition, the grain boundaries were less defined with the appearance of micropores and cracks, as shown in Fig. S2c, d, which can because that the excessive hBN tend to accelerate the thermal energy transfer, leading to the partial melting of the grains. As a result, as plotted in Fig. S2e, f, the mean grain diameters and the densities of the samples initially increased with increasing hBN additions owing to the improved grain growth, and then decreased with the increased contents above 0.2 wt.% of the hBN due to the partial melting of the grains, as can be seen in Fig. S1g, h.

Fig. S3 shows the Raman spectra of the resulting samples with various content of hBN, for all samples peaks at 75, 129, 239, and 446 cm⁻¹ that belong to the excited bands of the PMN-PMS-PZT matrix were observed throughout the whole range of the wavenumbers, as shown in Fig. S3a. As shown in Fig. S3b, the Raman peaks at 75 cm⁻¹ appeared without any shift, suggesting that addition of hBN did not affect the crystal structure of the PMN-PMS-PZT matrix. Meanwhile, the broadening of the full width at half maximum (FWHM) of the peak at 75 cm⁻¹ was initially observed with an increased hBN content due to grain growth [23], as shown in Fig. S3c. However, the FWHM decreased when the hBN content was beyond 0.2 wt.%, which can be ascribed to the increased micropores and cracks in the sample and the intensity of the peak continued to decrease as a function of hBN content, as shown in Fig. S2c, d.

The elemental distribution of the PMN-PMS-PZT: xhBN sample with x=0.1 is shown in Fig. 1c-f. The backscattered SEM images are presented in Fig. 1c, and the corresponding two-dimensional element maps are shown in Fig.1d-f and Fig. S3e, f. Fig. 1g shows the EDS spectrum of the PMN-PMS-PZT with 0.1 wt.% hBN. As clearly shown in Fig. 1d, the Pb distributed in the main area the sample while the Zr (Fig. S3e) appeared at the boundaries of the grains. For the other elements with lower atomic weight, such as B, N, and O, were uniformly dispersed in the ceramic matrix without any agglomeration as shown in Fig. 1e, f and Fig. S3f. Noticeably, the element B, unlike Al as discussed in our previous work [23], was homogenously distributed in the sample, which suggested the hBN filler was evenly distributed into the ceramic matrix of the PMN-PMS-PZT matrix, rather than being concentrated at the grain boundaries. As seen

in the EDS spectrum of Fig. 1g, all elements of the sample were detected, and the peaks of B and N were observed at 0.18 and 0.39 keV, indicating the existence of BN.

The temperature behavior of the relative permittivity (ε_r) and dielectric loss (tan δ) measured at 1 kHz over the temperature range between 25 and 300 °C with various hBN contents are illustrated in Fig. 2a, b, and the temperature behavior of the ε_r and tanδ of the sample with 0.1 wt.% hBN measured at various frequencies from 1 kHz to 1 MHz are shown in Fig. 2c, d. In general, the ε_r for each sample increased until 213 °C, and then decreased with an increase in temperature, suggesting a comparable Curie temperature (T_c) associated with a phase transition. As shown in Fig. 2a, the smallest ε_r was obtained by the sample with 0.1 wt.% hBN when the temperature was below 95 °C, which was possibly ascribed to the maximum density caused by the enhanced crystallinity of this composite. Since the figure of merit (FoM) for pyroelectric energy harvesting is $F_E = \frac{p^2}{\mathcal{E}_0 \mathcal{E}_c}$ [41], a relatively lower permittivity is beneficial for enhancing the performance of pyroelectric energy harvester. In contrast to the ε_r , the $\tan \delta$ for each sample was generally less than 0.02 when the temperatures were below 100 °C, as shown in the inset of Fig. 2b, indicating a relatively low leakage current. In addition, with an increase in frequency, the ε_r was gradually decreased at each temperature (Fig. 2c), which can be induced by the presence of dominant frequencydependent dielectric relaxation polarization [42]. At a relatively high frequency, the contribution from the relaxation polarization to the ε_r gradually became minor due to slower response times for the change at a frequency point under the ac field, resulting in the decrease in ε_r with the increased frequency [43]. Similarly, a decrease in tan δ was observed with an increase in frequency from 1 kHz to 1 MHz, as shown in Fig. 2d, since tanδ is inversely proportional to the frequency according to Debye relaxations [42].

The polarization-electric field (P-E) hysteresis loops of PMN-PMS-PZT: xhBN samples measured at room temperature, and the corresponding saturation polarization $(P_{\rm S})$ and remnant polarization $(P_{\rm r})$ are summarized in Fig. 3. Table S1 lists the specific values of the P_S and of P_r at each hBN concentration. Each sample similarly exhibits ferroelectric properties, which gradually varied with hBN contents. The peak value of the P_S of the samples initially increased from 23.9 to 36.4 μ C/cm² with 0.1 wt.% hBN, as shown in Fig. 3b and Table S1. The number of grain boundaries of lower permittivity was reduced and domain motion was less restricted as a result of an increased grain size [23, 44], this resulted in an enhanced polarization under an identical electric field for large grained materials. However, given that the presence of defects and the nonferroelecric filler gradually increased with a further increase in hBN content, domain switching became more difficult [45], leading to a slight decrease in P_S , as shown in Fig. 3b. Similarly, for the 0.1 wt.% hBN composite, the P_r increased from 13.1 to 17.7 μC/cm² owing to the enhanced polarization, and then gradually decreased when the hBN content increased beyond 0.1 wt.% (Fig. 3b). In particular, as shown in Table S1, only a minor decrease in the P_r was observed from 17.7 to 17.2 μ C/cm² when the content of hBN increased to 0.2 wt.%, which can be attributed to the effect of pinning forces on domains switching due to defects in the sample [23, 45]. Therefore, the addition of a small amount of hBN can effectively enhance the ferroelectric properties, and the

optimum $P_{\rm S}$ and $P_{\rm r}$ was achieved for a 0.1 wt.% hBN content. The coercive field ($E_{\rm c}$) was also sensitive to the hBN content, as shown in inset of Fig. 3a. When the hBN content increased from 0 to 0.2 wt.%, the $E_{\rm c}$ increased from 12.2 to 15.6 kV/cm, which can be due to the increased electic field for the $P_{\rm r}$ domains to reverse owing to the domain walls pinned by the hBN additions [46]. The $E_{\rm c}$ decreased to 14.6 kV/cm at 0.3 wt.%, possibly due to the increased defects (Fig. S2d).

The mechanism of pyroelectric effect is illustrated in Fig. 3c. At a steady state (dT/dt=0), the P_S remains constant and therefore no current is observed, however, as temperature increases (dT/dt>0), the ferroelectric dipoles move from their equilibrium position, leading to a decrease in P_S . Therefore, the current flows through the ammeter as shown in Fig. 3c. The pyroelectric coefficient (p) in a temperature range between 28 and 65 °C and the peak values of p as a function of hBN content are presented in Fig. 3d and Fig. 3e, respectively. The p increased in accordance with the P_S as a function of the hBN content, where p intiailly increased from 2947 to 3423 μ C/m²·K for 0.1 wt.% hBN, and then decreased to 2190 μ C/m²·K when the hBN content was 0.3 wt.%, as shown in Fig. 3e and Table S1. In addition, as shown in the inset of Fig. 3d, the peak positions of the p for the sample with 0.1 wt.% was similar (~ 33.3 °C) with that of the pristine PMN-PMS-PZT sample, and the peak position of p gradually shifted to higher temperatures with an increased hBN content, which can be due to changes in the microstructures of the samples as can be seen in Fig. 1a, b and Fig. S2c, d.

The simulation model of the pristine and the sample with addition of 0.1 wt.% hBN is shown in Fig. 4a. According to this hypothesis and Maxwell theoretical model [47],

the thermal conductivity can be calculated from the Equation (1):

$$K_{e} = K_{c} \left[\frac{K_{d} + 2K_{c} + 2\phi(K_{d} - K_{c})}{K_{d} + 2K_{c} - \phi(K_{d} - K_{c})} \right]$$
(1)

Where $K_{\rm e}$, $K_{\rm c}$ and $K_{\rm d}$ are the thermal conductivities of the composite, the continuous phase (the pure ceramic) and the discrete phase (the hBN), respectively. ϕ is the volume fraction of discrete phase. According to equation (1), the theoretical thermal conductivities are shown in Fig. S4a. In order to evaluate the real thermal conductivity (K), a laser flash analysis (LFA427) was used to measure the α . Fig. 4b shows the real K of all samples with various hBN contents from 25 to 60 °C, and the values of K for the samples at a temperature of 30.3 °C are shown in Fig. 4c. As seen in Fig. 4b, a slight decrease in the K was observed for each sample with an increase in temperature. With an elevated temperature, the thermal resistance [35] gradually increases due to the enhanced phonon scattering, resulting in the decrease of the K. Meanwhile, the addition of a hBN filler with a relatively faster thermal response can be an effective approach to enhance the thermal conduction of the ceramic matrix, which resulted in an increase of the K from 0.795 to 1.038 W/m·K at 30.3 °C when the hBN content increased from 0 to 0.3 wt.%, as shown in Fig. 4c. Namely, the formation of the PMN-PMS-PZT: xhBN hybrid ceramics can be a promising approach to achieve a higher thermal conductivity compared to the pristine ceramic.

Comparing the simulated result and the real data, it can be seen that the former is slightly less than the latter, since in the real materials the addition of hBN not only increased the effective K, but also changed the density and microstructure of the samples. Therefore, the measured K was used in the following simulation model. To

predict the thermal response of the proposed pyroelectric energy harvesters, we simulated a simplified heat transfer model with a 310 µm pyroelectric layer initially at 20 °C and a thermal boundary condition of 50 °C applied to opposing surfaces, while the resulting temperature change with time was monitored in the material. A heat capacity of C_p =290 J/kg°C was used, with a thermal conductivity of K = 0.795, 0.895, and 1.038 W/m·K for the samples with 0, 0.1 and 0.3 wt.% hBN at 30.3 °C, respectively. In addition, a mass density of $\rho = 7350$, 7550 and 7050 kg/m³ for the samples with 0, 0.1 and 0.3 wt.% hBN in the finite element analysis. The temperature distribution of the pure and the samples with 0.1 and 0.3 wt.% hBN calculated by Multiphysics ANSYS software at the same time interval are illustrated in Fig. 4d and Fig. S4b, respectively. It can be clearly seen that as more hBN is added to the samples, the higher the temperature increase. Fig. S4c shows the temperature in the sample center with time for the three materials for the boundary conditional and materials properties described above, where the sample with 0.3 wt.% hBN has the highest heating rate for a given thermal input compared with the other two materials. This can be explained that, with an identical thermal condition, the sample with 0.3 wt.% hBN will heat up more rapidly since it has the lowest density and thermal mass.

Fig. 5 shows the energy harvesting of the PMN-PMS-PZT: xhBN ceramics subjected to periodic temperature variations between 20 and 50 °C. The data was acquired from measurement system and the corresponding equivalent harvesting circuit (Fig. S5). Fig. 5 shows the rate of temperature change and the output voltage of all devices, and the corresponding values for the devices with various hBN contents are summarized in

Table S2. The cyclic changes in temperature and the rate of temperature change (dT/dt)of the pyroelectric energy harvester for the sample with 0.1 wt.% hBN content are shown in Fig. 5a and Fig. 5b, respectively. Under the forward connection, a positive output voltage pulse with 9.2 V was obtained, and the current was 0.92 µA with a load resistor of $10 \text{ M}\Omega$ (Fig. 5c, d). Under the reversed connection, the corresponding signals were inverted with the identical absolute value of that under forward connection as shown in Fig. 5e, f. A similar trend was also observed for each sample with cyclic temperature variations from 20 to 50 °C, as shown in Fig. S7. In order to have a better comparison for energy harvesting, each sample was fabricated with an identical thickness of 310 µm and a diameter of 8.5 mm (Fig. S6). With a 0.1 wt.% hBN addition, the peak value of the dT/dt increased by 8.15% from 3.19 to 3.45 °C/s (Table S2), indicating a more sensitive pyroelectric response. Correspondingly, the output voltage and current increased by 28.7% to 9.20 V and 0.92 µA when the hBN content was 0.1 wt.% compared to that of the device with the pristine ceramic. Subsequently, with a further increase in hBN content, the dT/dt gradually decreased. The dT/dt finally declined to 3.13 °C/s, which can be a result of the excessive defects in the ceramics. The variation of the peak output voltage (U) and the dT/dt for all devices are shown in Fig. 5g. Accordingly, a similar decrease trend in the output current (I) was observed with a further increase in hBN content (Table S2). As a result, based on the power, $P_{\rm E}=UI$, the maximum output power can be obtained with the 0.1 wt.% hBN sample, which is an increase of 65.6% compared to the device from the pristine PMN-PMS-PZT ceramic. The trend can be seen in Fig. 5h, suggesting that the addition of hBN

nanosheets can effectively enhance the heat transfer for pyroelectric energy harvesting applications.

4. Conclusion

In summary, we have designed and prepared new hybrid pyroelectric ceramics with high thermal conductivity hBN filler additions to a PMN-PMS-PZT ferroelectric ceramic to create PMN-PMS-PZT: xhBN composites. Detailed microstructural analysis substantiates that the hBN nanosheets were evenly distributed in the PMN-PMS-PZT matrix. The hybrid ceramic with 0.1 wt.% hBN exhibited improved ferroelectric and pyroelectric properties, and enhanced thermal conductivity compared to the PMN-PMS-PZT, which revealed the advantages of hBN additions in heat transfer and energy harvesting applications. Finally, we successfully harvested the heat energy from the pyroelectric energy harvesters with all the ceramics at forward and reversed connection to the measurement system. Compared to the pyroelectric energy harvester with 0 wt.% hBN nanosheets, the composite device based on a 0.1 wt.% hBN content produced 8.46 μW, which was a 65.6% increase in contrast to that of the device with 0 wt.% hBN content. The results confirmed the benefits of the designed hybrid pyroelectric ceramics, as predicted by theoretical derivations. This approach to the design of pyroelectric ceramics provides a route to enhance the heat transfer, microstructure and electrical properties to improve energy harvesting performance of pyroelectric harvesters, and represents a progress towards effectively utilizing ambient thermal energy as a source for self-powered devices and wireless sensor networks.

Acknowledgements

This work was supported by the National Science Foundation of China (Grant Nos. U1532146, 61675076, 61705070, 51672092, and U1732117), the China Postdoctoral Science Foundation (Grant Nos.2017M612449 and 2017T200545), the Natural Science Foundation of Hubei Province of China (Grant No.2016CFB533) and Wuhan Morning Light Plan of Youth Science and Technology (No.2017050304010299). We also would like to acknowledge the Analytical and Testing Center of Huazhong University of Science and Technology.

References

- [1] S. Chu, A. Majumdar, Nature 488 (2012) 294-303.
- [2] D. A. King, Science 303 (2004) 176-177.
- [3] N. Zhang, J. Chen, Y. Huang, W. Guo, J. Yang, J. Du, X. Fan, C. Tao, Adv. Mater. 28 (2016) 263-269.
- [4] J. Chen, G. Zhu, W. Yang, Q. Jing, P. Bai, Y. Yang, T. Hou, Z. L. Wang, Adv. Mater. 25 (2013) 6094-6099.
- [5] J. Chen, Z.L. Wang, Joule 1 (2017) 480-521.
- [6] Y. Ji, K.Zhang, Y. Yang, Adv. Sci. 5 (2018) 1700622.
- [7] K. Song, N. Ma, Y. Yang, Adv. Mater. Technol. 2 (2017) 1700221.
- [8] S. Wang, Z.L. Wang, Y. Yang, Adv. Mater. 28 (2016) 2881-2887.
- [9] K. Zhao, B. Ouyang, Y. Yang, iScience 3 (2018) 208-216.
- [10] Y. Yang, H. Zhang, X. D. Zhong, F. Yi, R. Yu, Y. Zhang, Z. L. Wang, ACS Appl. Mater. Interfaces 6 (2014) 3680-3688.
- [11] D. Kraemer, B. Poudel, H. Feng, J. C. Caylor, B.Yu, X.Yan, Y. Ma, X. Wang, D. Wang, A. Muto, K. McEnaney, M. Chiesa, Z. Ren, G. Chen, Nat. Mater. 10 (2011) 532-538.
- [12] Y. Zi, L. Lin, J.Wang, S.Wang, J. Chen, X. Fan, P. Yang, F. Yi, Z.L. Wang, Adv. Mater. 27 (2015) 2340-2347.
- [13] J. Chen, Y. Huang, N. Zhang, H. Zou, R. Liu, C. Tao, X. Fan, Z.L. Wang, Nat. Energy 1 (2016) 16138.
- [14] N. Ma, Y. Yang, Nano Energy 40 (2017) 352-359.
- [15] Y. Yang, Y. Zhou, J. Wu, F. Yi, Z.L. Wang, ACS Nano 6 (2012) 8456–8461.
- [16] C. R. Bowen, M. H. Arafa, Adv. Energy Mater. 5 (2015) 1-17.
- [17] G. Vats, A. Kumar, N. Ortega, C. R. Bowen, R. S. Katiyar, Energy Environ. Sci. 9 (2016) 2383-2391.
- [18] T. Park, J. Na, B. Kim, Y. Kim, H. Shin, E. Kim, ACS Nano 9 (2015) 11830-11839.

- [19] N. Ma, K. Zhang, Y. Yang, Adv. Mater. 29 (2017) 1703694.
- [20] K. Zhang, S. Wang, Y. Yang, Adv. Energy Mater. 7 (2017) 1601852.
- [21] Y. Wu, X. Wang, Y. Yang, Z. L. Wang, Nano Energy 11 (2015) 162-170.
- [22] S. Pandya, J. Wilbur, J. Kim, R.Gao, A. Dasgupta, C. Dames, L. W. Martin, Nat. Mater. 17 (2018) 432-438.
- [23] Q. Wang, C. R. Bowen, W. Lei, H. Zhang, B. Xie, S. Qiu, M. Li, S. Jiang, J. Mater. Chem. A. 6 (2018) 5040-5051.
- [24] Q. Wang, X. Zhang, C. R. Bowen, M. Li, J. Ma, S. Qiu, H. Liu, S. Jiang, J. Alloys. Compounds. 710 (2017) 869-874.
- [25] X. Lei, X. Dong, C. Mao, Y. Chen, F. Cao, G. Wang, Appl. Phys. Lett. 101 (2012) 262901-262904.
- [26] S. Jiang, P. Liu, X. Zhang, L. Zhang, Q. Li, J. Yao, Y. Zeng, Q. Wang, G. Zhang, J. Alloys. Compounds. 636 (2015) 93-96.
- [27] M. Xie, D. Zabek, C. R. Bowen, M. Abdelmageed, M. Arafa, Smart Mater. Struct. 25 (2016) 1-8.
- [28] A. Siao, C. Chao, C. Hsiao, Sensors-basel 15 (2015) 19633-19648.
- [29] A. Siao, C. Chao, C. Hsiao, Sensors-basel 16 (2016) 1-13.
- [30] C. Hsiao, A. Siao, Sensors-basel 13 (2013) 12113-12131.
- [31] D. Zabek, J. Taylor, E. L. Boulbar, C. R. Bowen, Adv. Energy Mater. 5 (2015) 1401891-1401896.
- [32] C. Hsiao, S. Liu, A. Siao, Sensors-basel 15 (2015) 16248-16264.
- [33] Z. Hana, A. Fina, Prog. Polym. Sci. 36 (2011) 914-944.
- [34] T. M. Tritt, Thermal conductivity: theory, properties, and applications, Kluwer Academic/Plenum Publishers, New York 2004.
- [35] I. Jo, M.T. Pettes, J. Kim, K. Watanabe, T. Taniguchi, Z. Yao, L. Shi, Nano Lett. 13 (2013) 550-554.
- [36] C. Zhang, X. Yao, Y. Lia, H. Liang, J. Chen, J. Zhang, J. Yang, X. Li, T. Qiu, Z. Chen, X. Liu, Z. Huang, Ceram. Int. 41 (2015) 9107-9114.
- [37] S. Chung, J. Lin. Molecules 21 (2016) 670-680.
- [38] Y. Zhang, M. Xie, J. Roscow, Y. Bao, K. Zhou, D. Zhang, C. R. Bowen, J. Mater. Chem. A 5 (2017) 6569-6580.
- [39] A. L. Cottrill, A. T. Liu, Y. Kunai, V. B. Koman, A. Kaplan, S. G. Mahajan, P. Liu, A. R. Toland, M. S. Strano, Nat. Commun. 9 (2018) 1-11.
- [40] C. Xu, M. Miao, X. Jiang, X. Wang, Compos. Commun. 10 (2018) 103-109.
- [41] C. R. Bowen, J. Taylor, E. LeBoulbar, D. Zabek, A. Chauhan, R. Vaish, Energy Environ. Sci. 7 (2014) 3836-3856.
- [42] M. Sudipta, D. C, V. A, T. D, Appl. Phys. Lett. 111 (2017) 1-4.
- [43] D. Choudhury, P. Mandal, R. Mathieu, A. Hazarika, S. Rajan, A. Sundaresan, U. V. Waghmare, R. Knut, O. Karis, P. Nordblad, D. D. Sarma, Phys. Rev. Lett. 108 (2012) 1-5.
- [44] L. Zhang, S. Jiang, Y. Zeng, M. Fu, K. Han, Q. Li, Q. Wang, G. Zhang, Ceram. Int. 40 (2014) 5455-5460.
- [45] Y. Tang, P. Li, W. Zhang, H. Ye, Y. You, R. Xiong, J. Am. Chem. Soc., 139 (2017) 13903-13908.

- [46] B. Hanrahan, L. Sanchez, C. M. Waits, R. G. Polcawich, Smart Mater. Struct. 25 (2016) 015025-015034.
- [47] R. C. Progelhof, J. L. Throne, R. R. Ruetsch, Polym. Eng. Sci. 16 (1979) 615-625.



Qingping Wang received her Ph.D. degree in Electronic Science and Technology from Huazhong University of Science and Technology (HUST) in 2018. She is an associate professor in Hubei University of Education. Her current research interest is pyroelectric energy harvesting based on nanomaterials and ceramic materials.



Christopher Rhys Bowen has a BSc degree in Materials Science from the University of Bath (1986-1990) and a Ph.D. in Ceramics from the University of Oxford (1990-1993). Post-doctoral work has been undertaken at Tecnische Universität Harburg-Hamburg and University of Leeds (1994-1996). He was Senior Scientist at the Defence Evaluation and Research Agency from 1996-1998. He joined the University of Bath as a Lecturer in 1998 and is now Professor of Materials. Research areas include energy harvesting, piezoelectric materials, dielectrics and functional ceramics.



Rhodri Wyn Charles Lewis has a BEng degree in Sports Engineering (2003-2007) and

a Ph.D. in Piezoceramics from the University of Bath (2007-2011). Post-doctoral research into the fabrication of highly ordered nanostructures was undertaken at the University of Bath (2010-2012). He joined Renishaw Plc in 2012 and is now a Materials Scientist working in research and development with interests in piezoelectric devices (ultrasonics and energy harvesting) and additive manufacturing.

.



Dr. Jun Chen is currently a postdoctoral research fellow with Prof. Yi Cui at Stanford University. He received his Ph.D. in Materials Science and Engineering from the Georgia Institute of Technology in 2016 under the supervision of Prof. Zhong Lin Wang. His research focuses on nanotechnology for energy, sensors, healthcare, and environment in the form of smart textile, wearables, and Internet of things. He has already published 2 books, 86 journal articles and 46 of them are as first/corresponding authors in Nature Energy, Nature Sustainability, Nature Communications, Joule, and many others. His current h index is 53.



Lei Wen obtained his Ph.D. degree in Materials from Huazhong University of Science and Technology (HUST) in 2008, he is a professor at School of Optical and Electronic Information in HUST. His research activities are mainly concerned with microwave dielectric materials and devices for microwave communication. He has undertaken more than 10 research projects supported by the National Natural Science Funds and National Defense Basic Scientific Research, etc. And about 70 academic papers have

been published and several research productions have been applied successfully for antenna, resonator and LTCC.



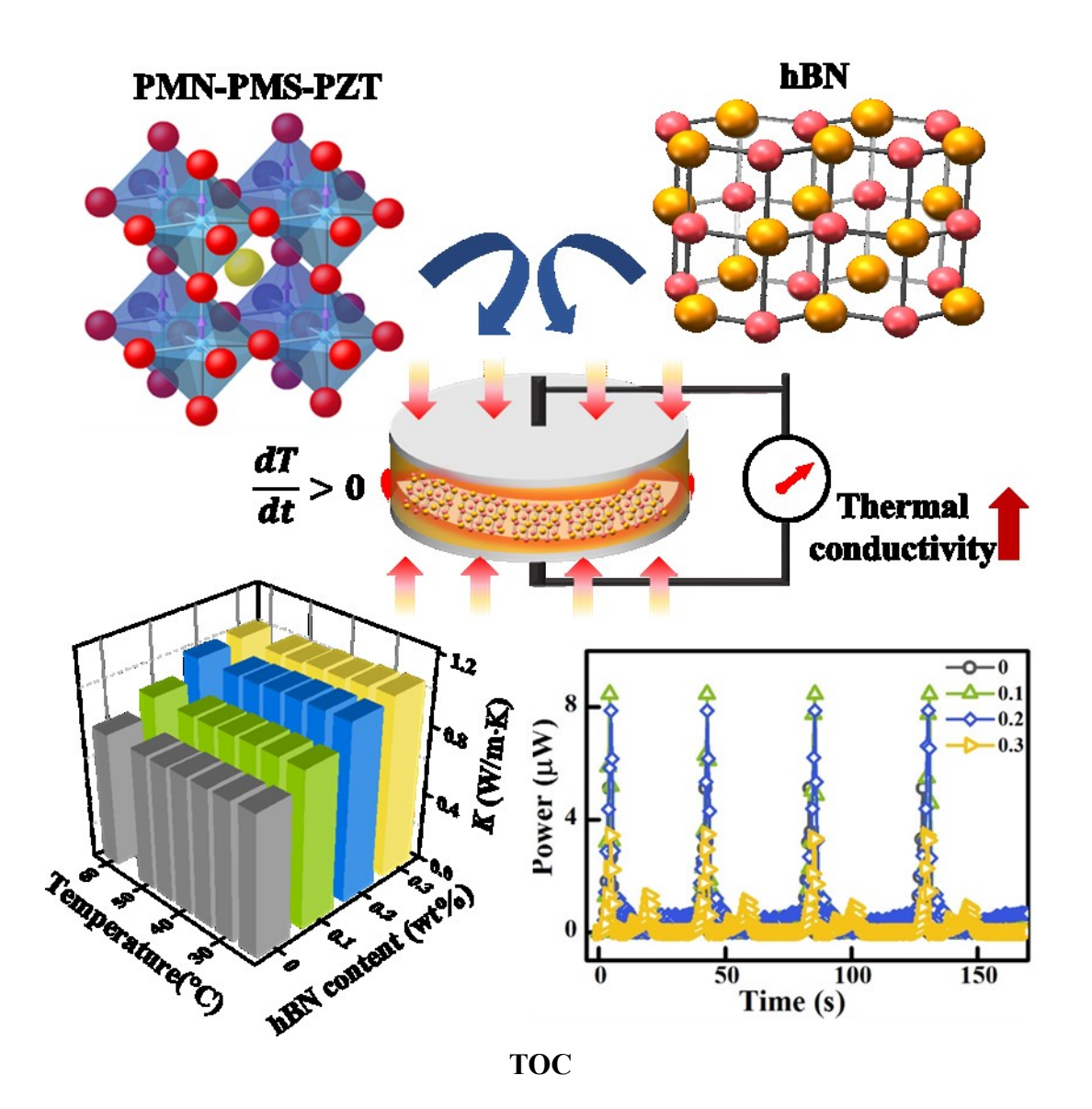
Haibo Zhang obtained his Ph.D. degree from Huazhong University of Science and Technology (HUST) in 2008. He had been a postdoctoral researcher for two and a half years in Kochi University, Japan. Zhang got a faculty position in School of Materials Science and Engineering at HUST in 2011. From 2012 to 2014, he worked as a Humboldt Research Fellow with Professor Jürgen Rödel in University of Darmstadt, Germany. Since 2014 he works as an associate professor in School of materials science and Engineering at HUST.



Ming-Yu Li received his Ph.D. degree in Electronic Engineering from Kwangwoon University, Korea in 2016. He is recently a postdoctoral fellow at Huazhong University of Science and Technology (HUST). His research interests focus on nanomaterials synthesize, nanostructures fabrication and characterization, functional materials and, energy devices. He serves as guest editor of MDPI Nanomaterials. He has published more than 50 research papers in international journals, and been authorized more than 4 international patents.



Shenglin Jiang received his Ph.D. degree in Microelectronics and Solid-State Electronics from Huazhong University of Science and Technology (HUST). He is a professor in School of Optical and Electronic Information at HUST. His research interests include the ferroelectric and dielectric materials and devices. He has published more than 103 research papers. He is the fellow of the Chinese Materials Research Society, Chinese Journal of Electronics, and the Photoelectronic Technology Professional Committee of the Chinese Society of Astronautics. For the details please check the lab website: http://www.afmd.oei.hust.cn.



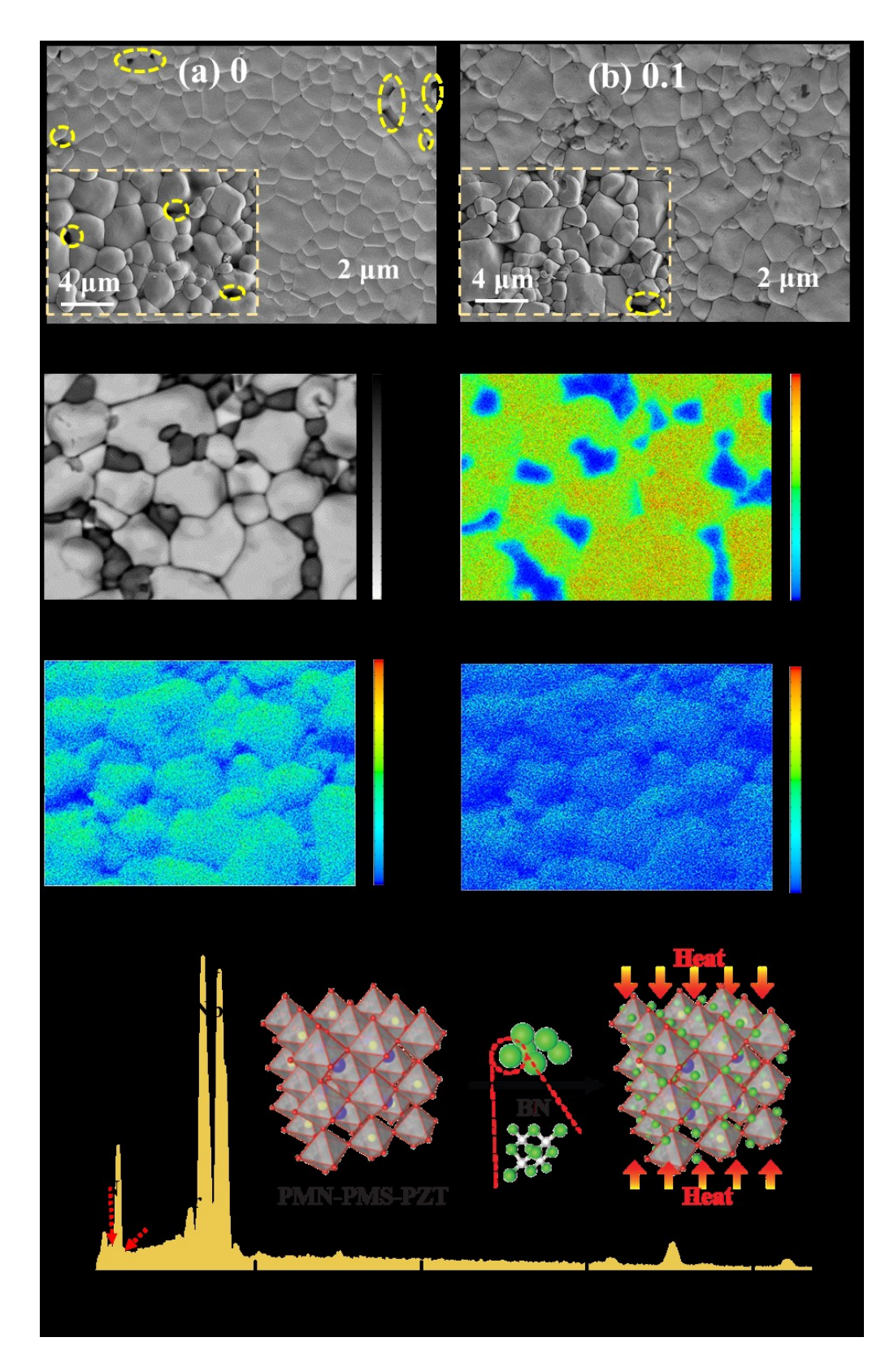


Fig. 1. SEM microstructures of samples, (a) x=0, (b) x=0.1, Microstructure image and corresponding elemental distribution including, (c) Composite (d) Pb, (e) B, and (f) N, (g) Energy-dispersive spectrum pattern recorded from the local area.

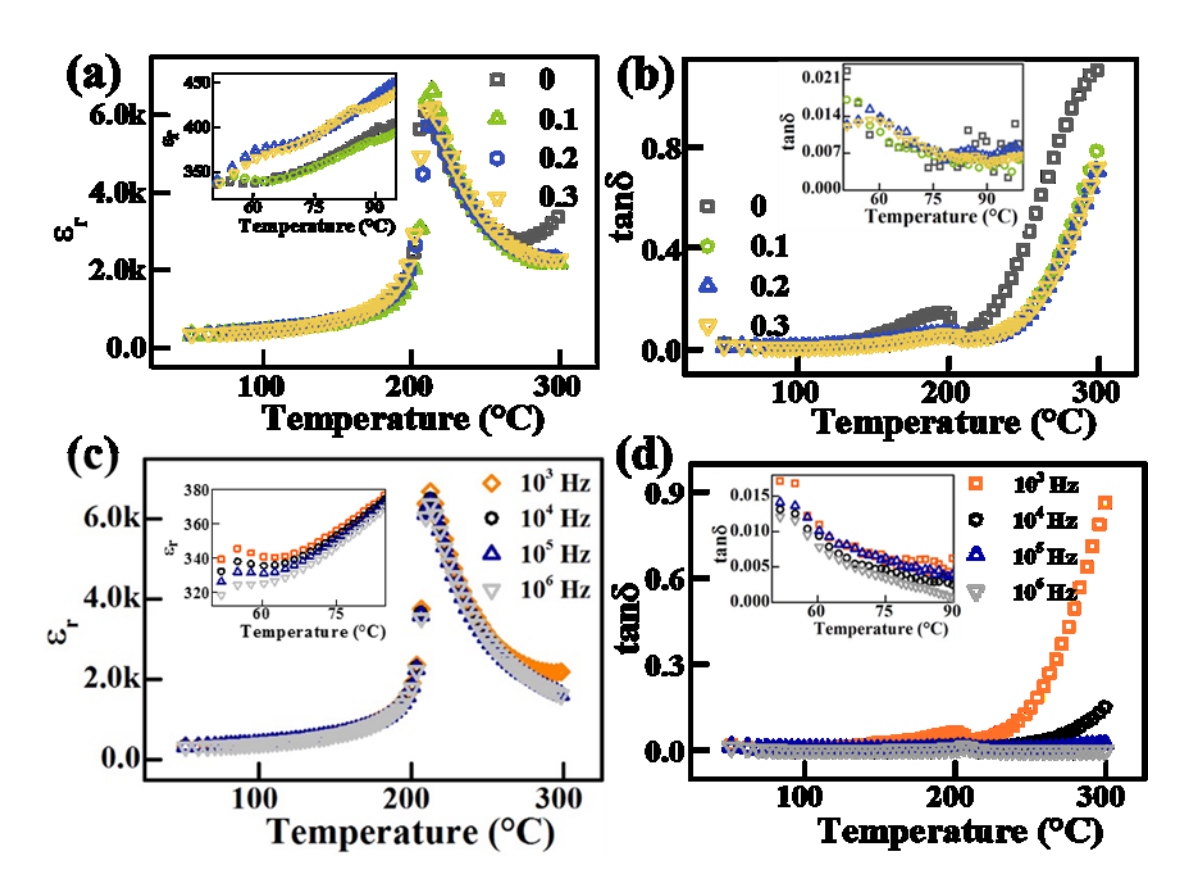


Fig. 2. Temperature dependent dielectric constant (a) and dielectric loss (b) of all samples. Temperature dependent dielectric constant (c) and dielectric loss (d) of sample with x=0.1 wt.% at different frequencies.

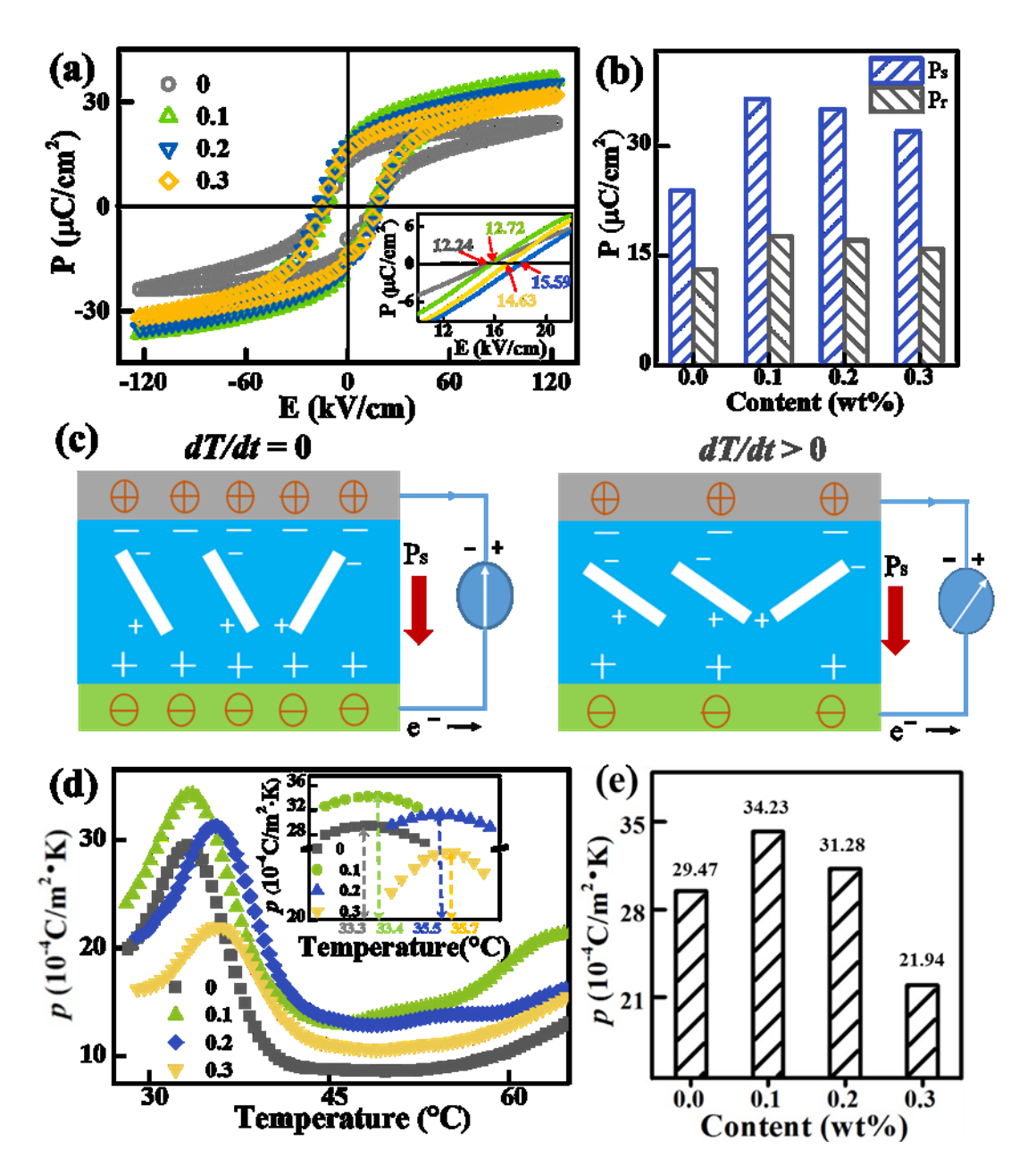


Fig. 3. (a) P-E loops and (b) P_s and P_r of samples with x=0~0.3, (c) Mechanism of pyroelectric effect, (d) Temperature dependent pyroelectric coefficient and (e) pyroelectric values of the corresponding samples.

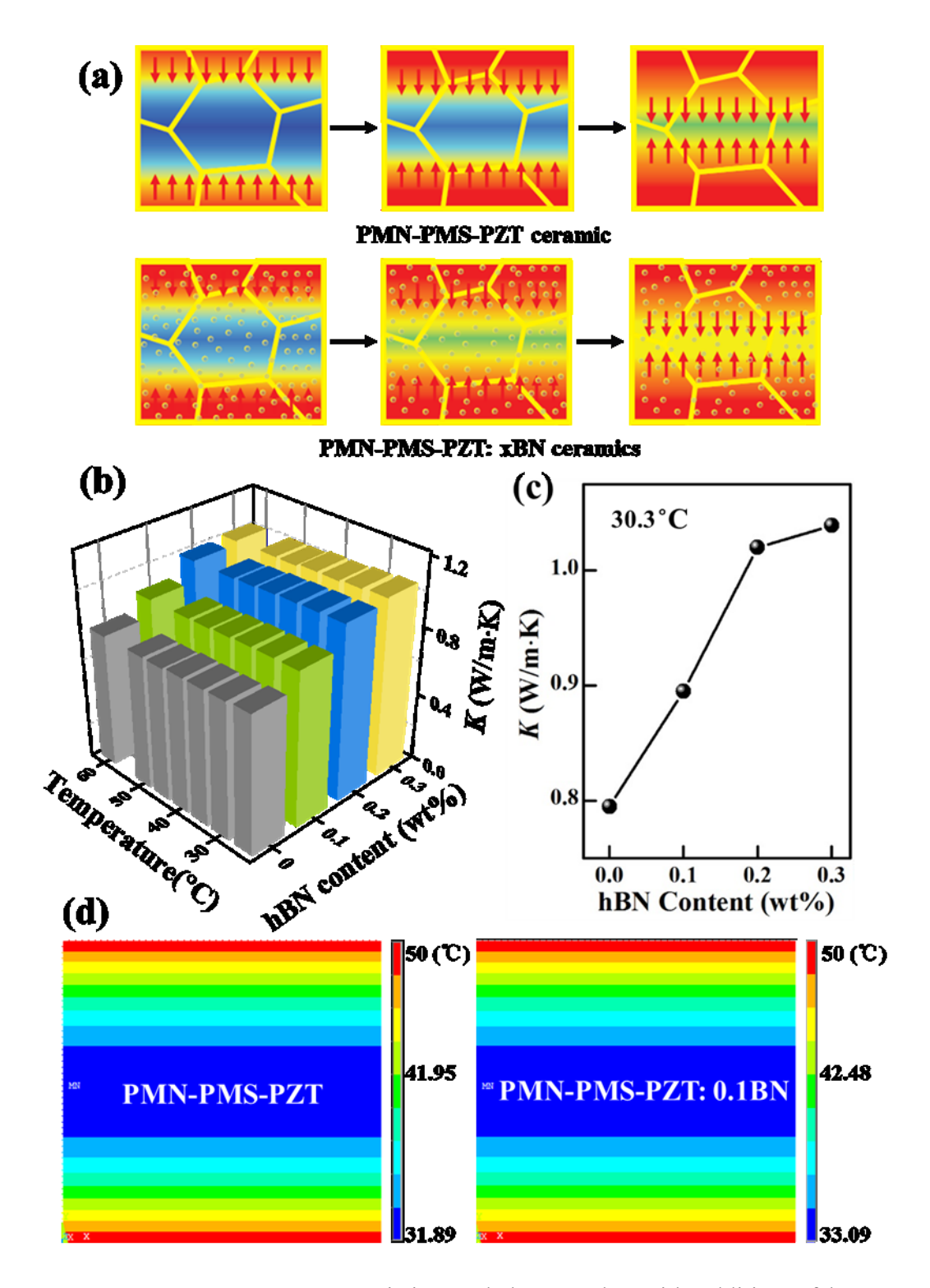


Fig. 4. (a) Simulation model of the pristine and the samples with addition of hBN, (b) Measured *K* as a function of temperature and BN content, (c) Detailed values of *K* with various BN contents, (d) Temperature distribution in the pristine and the sample with 0.1 wt.% hBN obtained from the ANSYS simulation.

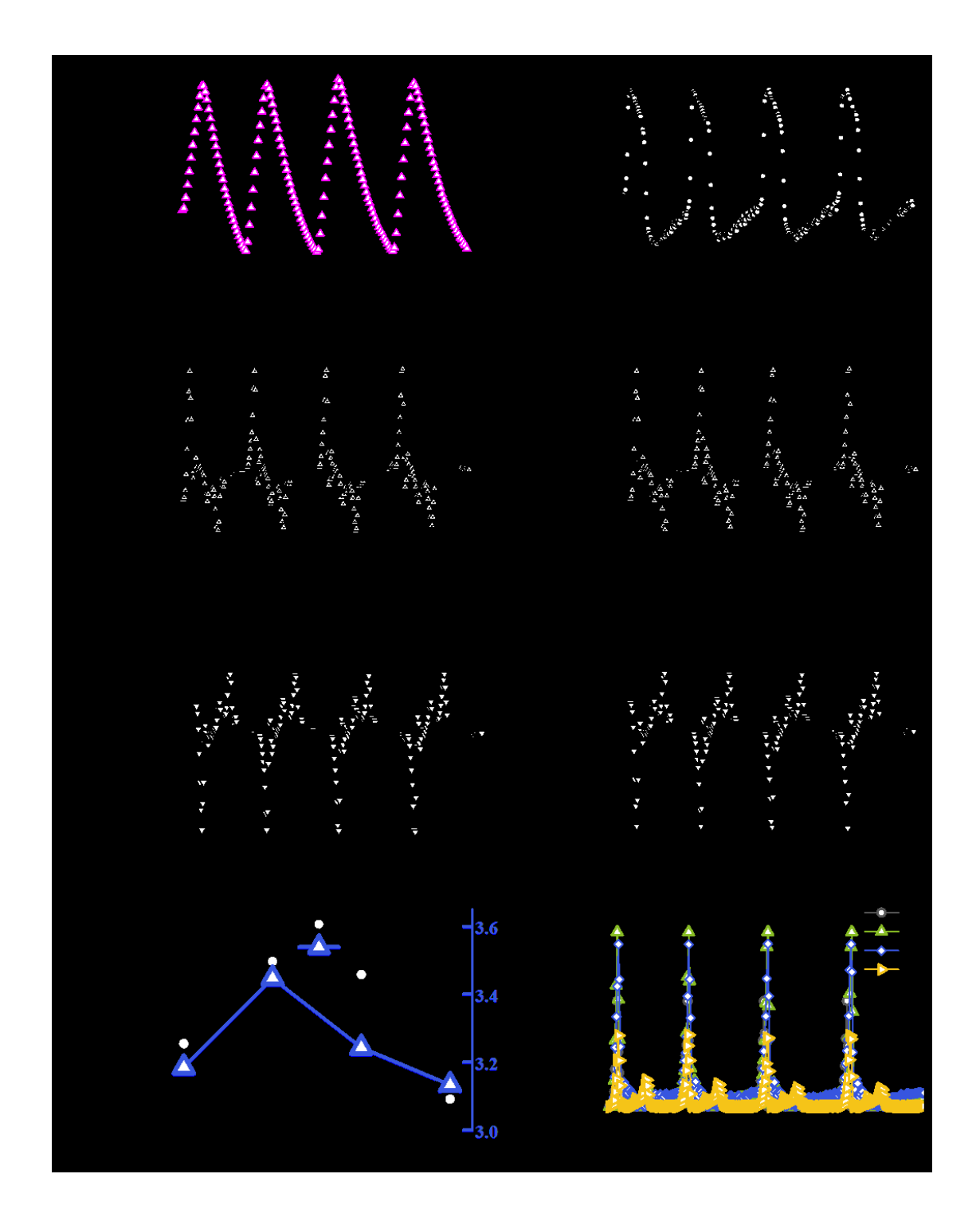


Fig. 5. (a) Cyclic changes in temperature and (b) the rate of temperature change, (c, d, e, f) Measured output voltage and current of the pyroelectric devices with the sample with 0.1 wt.% BN at forward connection and reversed connection to the measurement system, (g) Peak voltage, dT/dt and (h) power of all samples.